 Bull. Chem. Soc. Jpn. Vol. 80, No. 4, 637–648 (2007)

Award Accounts

The Chemical Society of Japan Award for Young Chemists for 2005

Atomic and Electronic Structures and Properties of Nanomaterials on Metal Substrates

Manabu Kiguchi

Department of Chemistry, Graduate School of Science, Hokkaido University, Sapporo 060-0810

Received July 26, 2006; E-mail: kiguti@sci.hokudai.ac.jp

We have fabricated well-defined nanostructures and investigate their chemical and physical properties. First, we studied atomic and electronic structures of alkali halide films grown on metal substrates. Alkali halides were found to grow heteroepitaxially on fcc metal (001) surfaces, that is, a well-defined insulator/metal interface could be prepared. We could obtain clear experimental evidence for the formation of metal-induced gap states at the interface using near edge X-ray absorption fine structure. Second, we fabricated a polar MgO(111) thin film by alternate adsorption of Mg and O_2 on Ag(111). The polar MgO(111) surface was not an insulating surface, but a semiconducting or metallic surface. Third, we studied the chemical and physical properties of these well-defined nanostructures. In case of monoatomic Au wires, we succeeded in controlling the switching behavior of conductance by the external perturbation, electrochemical potential.

1. Introduction

With a decrease in size or dimensionality of materials, various phenomena become observable. For example, Shockley and Tamm states are formed on a clean Cu surface.[1] Peculiar catalytic properties are observed for Au nanoparticles.[2] In order to investigate the low-dimensional materials, their atomic and electronic structures and chemical/physical properties should be studied at the same time.

In the present study, we studied the atomic and electronic structures and chemical and physical properties of low-dimensional materials. Especially, we paid attention to the two-dimensional material, hetero-interface. At the interface, one can prepare metastable structures, which closely imitate those of the substrates rather than the bulk equilibrium phase. The interatomic distance can be elongated by as large as ≈10% in some cases.[3–5] On the technological side, electronic devices, such as diode, transistor, laser, use the properties at the hetero-interface.[6,7] Among various hetero-interfaces, there has been a growing interest in the insulator/metal interface due to its importance in catalysis, device applications, and fundamental science. Insulators on metals are applied to gate insulators in miniaturized electronic circuits, and magnetic tunnel junctions for magneto electronics and magnetic data storage. Despite these interests, the insulator/metal interface has not been studied satisfactorily, for several reasons. First, well-defined interfaces have been hard to prepare due to the different nature of chemical bonds. Second, it is difficult to investigate the electronic structure of the interface, since signals from it are obscured by significant contribution from the substrate in conventional experimental methods.

In the present study, we discuss the fabrication of the well-defined an alkali halide/metal interface and observation of metal-induced gap states characteristic of the insulator (semiconductor)/metal interface in Section **2**. In Section **3**, we discuss the fabrication of a polar surface of metal oxides on metal substrates, and its electronic structure. We then discuss the chemical/physical properties of the well-defined nanomaterial. In Section **4**, we discuss the electrical conductance of organic films and a nanowire in solution.

2. Fabrication of a Well-Defined Insulator/Metal Interface and Observation of Metal-Induced Gap States

2.1 Fabrication of Well-Defined Insulator/Metal Interfaces. In order to fabricate a well-defined insulator/metal interface, we focused on alkali halides as an insulator for the following reasons. First, the wide range of lattice constants for alkali halide (from 0.40 nm (LiF) to 0.73 nm (RbI)) is advantageous for the heteroepitaxial growth, since matching of the lattice constant is important for the heteroepitaxial growth. Second, alkali halides can grow on alkali halides in a layer-by-layer fashion even with a lattice misfit as large as 20%, and at low substrate temperatures.[3–5] We have, thus, studied the thin film growth for various alkali halide(film)–metal(substrate) combinations. The systems investigated here were LiCl/Ni(001), LiCl/Ag(001), NaCl/Ni(001), NaCl/Cu(001), NaCl/Ag(001), and $NaCl_{0.6}Br_{0.4}$/Ag(001), where the difference in the first-nearest neighbor (NN) interatomic distance between alkali halide and metal were 2.9, −11.2, 13.2, 10.3, −2.4, and 0.0%, respectively.

The experiments were performed in a custom-designed ultrahigh-vacuum (UHV) system with a base pressure of

Published on the web April 13, 2007; doi:10.1246/bcsj.80.637

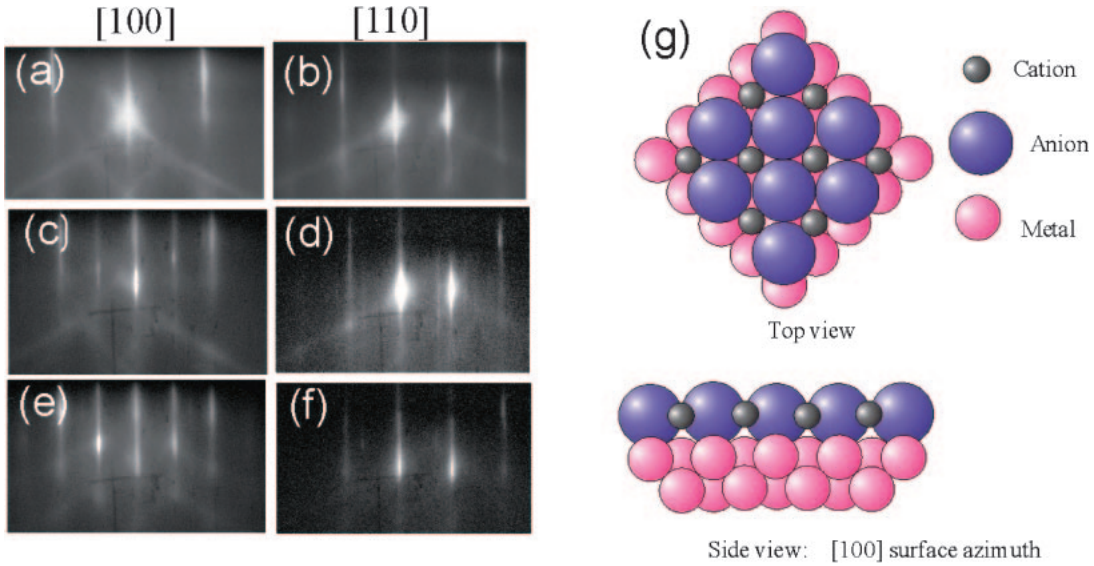

Fig. 1. A typical sequence of RHEED patterns during growth of LiCl on Cu(001) at the substrate temperature of 300 K. Film thickness were as follows: (a, b) 0 ML (Cu substrate), (c, d) 1 ML and (e, f) 20 ML. The incident beam was parallel to the [100] (a, c, e) or [110] (b, d, f) azimuth of the Cu(001) substrate. (g) The structure model of a 1 ML thick LiCl film on Cu(001) (Reprinted with permission from Ref. 10).

1×10^{-7} Pa. Mechanically and electrochemically polished Cu and Ni(001) crystals were cleaned by repeated cycles of Ar^+ sputtering and annealing at 900 K. The sample temperature was monitored with a chromel–alumel thermocouple, which was spot-welded onto a Ta sheet attached to the sample surface. After repeated preparation cycles, a sharp reflection high energy electron diffraction (RHEED) pattern was observed, and no contaminant was detected by Auger electron spectroscopy (AES). Alkali halide was evaporated from a Knudsen cell. The growth rate was monitored using a quartz crystal oscillator, and it was on the order of 1 ML (mono layer: ≈3 Å)/min. Real-time observation of crystallinity and orientation of films was done by RHEED. Surface atomic compositions of the deposited films were investigated in-situ by AES. The analyses were performed with a double pass CMA (PHI 15-255G) in the analysis chamber. Using a pulse counting detector, the probing electron current was reduced to 1 nA, which reduced surface damage as much as possible.[8]

Figures 1a–1f show the RHEED patterns during the growth of a LiCl film on a Cu(001) substrate at a substrate temperature of 300 K. The incident electron beam was parallel to the [110] or [100] azimuths of the substrates. As soon as the growth of LiCl began, the RHEED patterns changed into those of LiCl. The result of figures indicated that a single-crystalline LiCl film grew heteroepitaxially on a Cu(001) substrate. The streaks in the RHEED patterns showed that the film surface remained flat during growth, and layer-by-layer growth occurred from the initial stage. The layer growth was also supported by the Auger spectra. As can be seen in Fig. 1, the diffraction patterns taken along the [110] surface azimuth did not change, although half-order streaks appeared along the [100] surface azimuth. These RHEED patterns indicate that the in-plane lattice constant of the LiCl film was $\sqrt{2}$ times as large as that of the Cu substrate and that the LiCl islands were rotated by 45° relative to the Cu(001) substrate. This is because a 45° rotation reduces the misfit between LiCl and Cu(001) from 40 to 0.4%. Density functional calculations were performed for model clusters in order to investigate the interface structure. The LiCl island was adsorbed more stably on the fourfold hollow site of the first Cu layer than on the atop site. Figure 1g shows the structure of the model of LiCl/Cu(001) based on the RHEED and calculation results. It should be noted that this is the first experimental result of heteroepitaxial growth of alkali halide on metal substrates. By using alkali halide as an insulator, we could fabricate a well-defined insulator/metal interface.[9,10]

We then studied other combinations of alkali halide and metal. On Ni(001), LiCl also grew with its [100] axis rotated by 45° from that of the metal substrate ($[100]_{film}//[110]_{substrate}$). On the other hand, on Ag(001) and Cu(001), the alkali halides grew without azimuthal rotation ($[100]_{film}//[100]_{substrate}$) for LiCl/Ag(001), NaCl/Cu(001), NaCl/Ag(001), and $NaCl_{0.6}Br_{0.4}$/Ag(001). The former growth mode ($[100]_{film}//[110]_{substrate}$) occurred only with a small difference in the first-NN interatomic distance between alkali halide and metal and strong bonding between alkali halide and metal. The latter growth mode ($[100]_{film}//[100]_{substrate}$) occurred even with a large difference in the first-NN interatomic distance.

The latter growth mode is ascribed to the following growth mechanism based on the weak interaction between alkali halide and metal. First, although various steps might exist on a (001) face of an fcc crystal, every step can be thought to consist of two types of steps. Here, we define "(110) step," as the steps that is oriented in the [110] direction, and "(100) step" as the steps in the [100] direction (see Fig. 2a). The (110) step exposes a (111) face, while the (100) step exposes a (110) face. Since the (111) face is energetically more stable than the (100) face for fcc transition metals, a majority of the steps on the (001) surfaces of fcc transition metals are likely to be (110) steps. Second, conduction electrons do not follow entirely the short-range corrugation of the surface of the steps, and thus, the upper (lower) side of the step edge is positively (negatively) charged (Smoluchowski effect), as shown in Fig. 2b.[11]

When alkali halide molecules diffuse to the step sites, cations of alkali halide molecule adsorb preferentially at the negative lower side of the step edge, while anions adsorb preferentially at the positive upper side of the step edge. Therefore, cations (anions) align along the lower (upper) side of the (110) step, as shown in Fig. 2c. At the initial stage of the growth, alkali halide molecules are expected to adsorb following this rule. When the succeeding molecule comes to the initially adsorbed molecules, a rock salt lattice is formed with its [100] axis parallel to the [100] axis of the substrate.

In this section, we mainly discussed the growth of alkali halide on metal substrates. We have also fabricated a well-defined oxide film[12] and organic films[13–15] on metal substrates.

2.2 Observation of Metal-Induced Gap States at Alkali Halide/Metal Interfaces. We have been able to prepare well-defined insulator/metal interfaces, we then studied the electronic structure of the interfaces. To study the electronic structure, the detection method for characterizing the electronic structure of the interface is important. In conventional photoemission spectroscopy, signals from the interface are obscured by those from the substrate. In previous studies, we have employed ultraviolet photoemission spectroscopy and EELS to probe the LiCl/Cu(001) interface, however, states characteristic of the interface have not been obserbed.[16] Here, we have used X-ray absorption spectroscopy, which is chemical species-selective method.[17–20] The Cl K edge near edge X-ray absorption fine structure (NEXAFS) is based on the X-ray absorption of the Cl atom, and hence, provides information on the electronic structure of the alkali halide film (NaCl and LiCl) itself with negligible influence from the metal substrate. Furthermore, NEXAFS can even probe a deep interface, because the probing depth of NEXAFS with its high-energy photons (≈3000 eV) is ≈1000 nm. It can be used to obtain the dependence of the interface states on the insulating layer thickness. Therefore, NEXAFS is one of the most appropriate methods for studying the electronic structure at the insulator/metal interface.

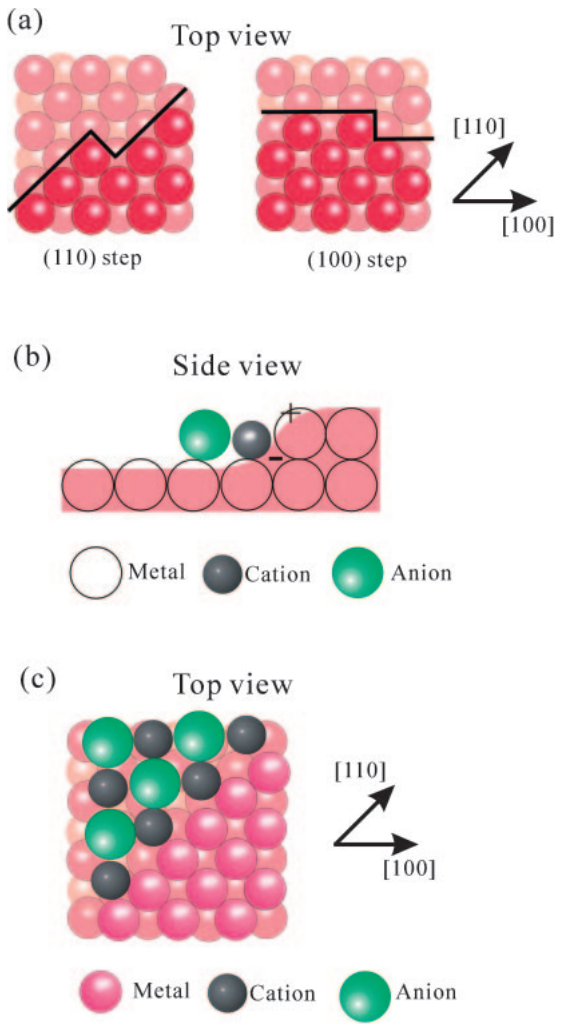

Fig. 2. (a) Schematic top view of steps on (001) surfaces of fcc transition metals; (110) step which orients in the [110] direction, and (100) step which orients in the [100] direction. (b) Basic model of the binding geometry. Because of the Smoluchowski smoothing effect, upper (lower) side of step edges is positively (negatively) charged. Cations adsorb at the lower side of step edges. (c) Sphere model of the alkali halide film grown on (001) face of the fcc transition metal. Cations align along the lower side of the (110) step (Reprinted with permission from Ref. 10).

Cl K edge NEXAFS measurements were carried out using the soft X-ray double-crystal monochromator station BL-11B of the Photon Factory at the High Energy Accelerator Research Organization.[21] The energy resolution of the Ge(111) monochromator was about 1.5 eV. The fluorescence yield detection method was employed to obtain NEXAFS data by using an UHV-compatible gas-flow proportional counter with P10 gas (10% CH_4 in Ar) as a detector.[22] The Cl1s X-ray photoemission spectrum (XPS) was measured using X-ray synchrotron radiation at 2900 eV with a RIGAKU XPS-7000 concentric hemispherical analyzer.

Figure 3 shows the Cl K edge NEXAFS spectra for LiCl/Cu(001) and LiCl/Ag(001) taken at grazing X-ray incidence for various thicknesses of the LiCl layer. All the spectra were

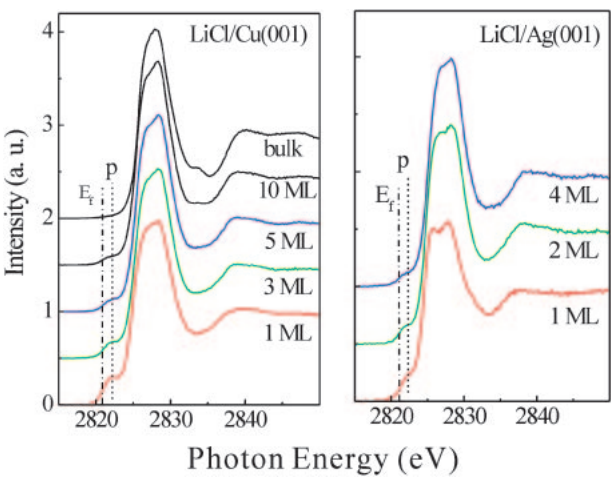

Fig. 3. The Cl K edge NEXAFS spectra in LiCl films grown on Cu(001) and Ag(001) for various thicknesses of the LiCl layer. All the spectra are normalized by their edge-jump, E_F indicates the position of the Fermi level as determined from XPS. The X-ray incidence angle is 15° (Reprinted with permission from Ref. 26).

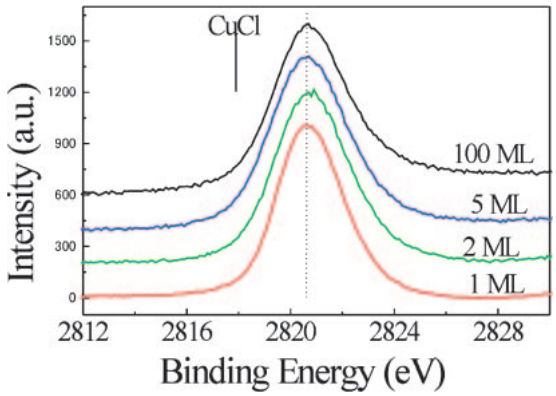

Fig. 4. The Cl1s XPS spectra in LiCl/Cu(001) for various thicknesses of the LiCl layer with a photon energy of 2900 eV. The binding energies are defined with respect to the Fermi level. For comparison, the binding energy of the bulk LiCl (dot line) and CuCl(line) crystal is shown in the figure (Reprinted with permission from Ref. 26).

normalized by their edge-jump. As the thickness of the LiCl layer was decreased, a pronounced pre-peak (p) emerged below the bulk edge onset. Since NEXAFS qualitatively provides information on the density of states of unoccupied states, the appearance of the pre-peak below the edge indicated the formation of new electronic states below the vacuum level and above the Fermi level in the LiCl films.

There are two points to note about the pre-peak. First, the pre-peak was observed even for the 10 ML LiCl on metal substrates. Since the electronic structure of a free-standing 1 ML film is different from that of a bulk crystal, a new electronic state can be formed apart from bulk band for the free-standing 1 ML film. Therefore, we could not find whether a state observed for a 1 ML film/metal system was characteristic of the interface or one was specific to 1 ML. The fact that the pre-peak was observed even for the thick film showed that the new state was characteristic of the interface. Second, the pre-peak was observed for both LiCl/Cu(001) and LiCl/Ag(001). Although the interface structure was different between LiCl/Cu(001) and LiCl/Ag(001) as discussed in the previous section, the pre-peak was observed in both systems. This indicated that the pre-peak did not originate from local structures at the interface.

To confirm whether the nature of chemical bonds was modified around the interface, we investigated the electronic structure of the LiCl film and the metal substrate with XPS and AES. Figure 4 shows the Cl1s XPS in LiCl/Cu(001) for various LiCl thicknesses. For comparison, the spectrum and the peak position of bulk LiCl and CuCl were also measured and indicated in the figure. The Cl1s binding energy of bulk CuCl was lower by 2 eV than that of bulk LiCl. If LiCl interacted with Cu to form a new chemical bond, i.e., Cl–Cu bond, at the interface, a satellite peak at the lower binding energy side or the broadening of the peak should occur. However, the binding energy and the half width of the Cl1s peak did not change with film thickness, nor did a satellite peak appear in LiCl/Cu(001), indicating that the chemical state of Cl in LiCl/Cu(001) was the same as that of bulk LiCl with no chemical bonds formed at the interface. The chemical state of Cu

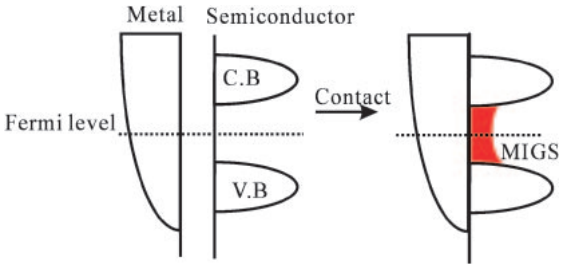

Fig. 5. Schematic view of MIGS at the semiconductor/metal interface. When a metal and a semiconductor contact, metal wave functions penetrate into the semiconductor side of the interface, and MIGS are formed in the band gap of the semiconductor.

was investigated using AES.[23] The Cu MMM AES peak, which was surface sensitive, did not shift from that of clean Cu(001) within 0.1 eV, indicating that the interfacial Cu atoms remained almost neutral. These results showed that no chemical bonds were formed at the interface.

Here, we summarize the above NEXAFS, XPS, and AES results. NEXAFS: A pre-peak was observed irrespective of the interface structure. XPS: The chemical state of Cl in LiCl/Cu(001) was the same as that of bulk LiCl. AES: The interfacial Cu atoms remained almost neutral for LiCl/Cu(001). These results clearly showed that the pre-peak observed by using NEXAFS originated not from local chemical bonds at the LiCl/metal interface, but from the states formed by proximity to a metal. The pre-peak could be assigned to metal-induced gap states (MIGS).

Here, we briefly explain MIGS at the insulator/metal interface.[24,25] At the semiconductor or insulator/metal interface, a free-electron-like metal wave function penetrates into a semiconductor (or insulator) side, and thus, the interface electronic states are formed in the band gap (see Fig. 5). These interface electronic states are MIGS. MIGS are considered to determine the Schottky barrier height at the semiconductor/metal interface, and thus, they are important electronic states. Despite the importance of MIGS, the existence of MIGS has not been proven to the best of our knowledge even at the semiconductor/metal interface, due to difficulty in the fabrication of the well-defined interface and the detection of the interface states. Unambiguous experimental evidence showed that MIGS were formed at atomically well-defined alkali halide/metal interfaces by using NEXAFS.[26,27]

The existence of the MIGS was also confirmed by using first-principles calculation based on the local density functional theory with pseudopotentials and plane-wave basis. The new in-gap states, of which the amplitude of the LDA wave functions reside on the Cl atoms and metal atoms at the interface, appeared for both LiCl/Cu and LiCl/jellium systems. The appearance of MIGS for LiCl on jellium showed that MIGS were characteristic of insulator/metal interfaces rather than from local modifications in the chemical bonds. Recently, MIGS were also observed for the epitaxially grown organic insulator film on metal substrates.[28]

2.3 Character of Metal-Induced Gap States at Alkali Halide/Metal Interfaces. As we have shown experimental and theoretical evidences for the formation of MIGS at alkali

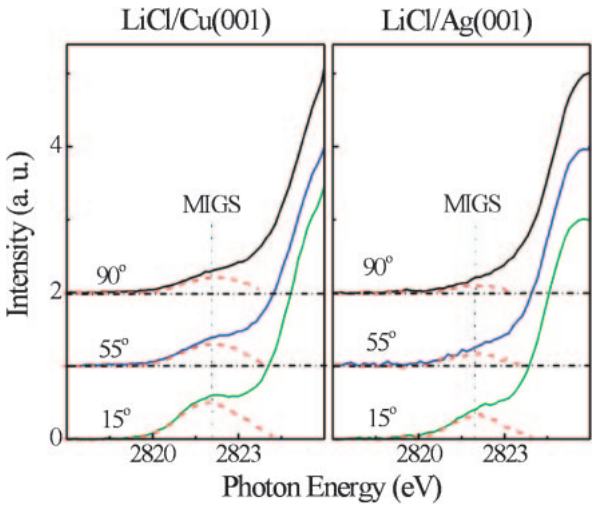

Fig. 6. Polarization dependence of the Cl K edge NEXAFS spectra for 1 ML LiCl/Cu(001) and 1 ML LiCl/Ag(001). The X-ray incidence angle is 15, 55, and 90°. The MIGS peaks are given as dot lines (Reprinted with permission from Ref. 26).

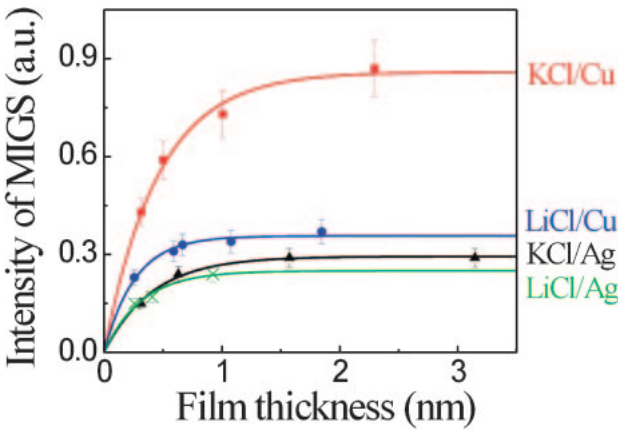

Fig. 7. The intensity of the pre-peak (not normalized by the edge-jump unlike in Fig. 3 versus the film thickness). The intensity of the pre-peak is obtained by subtracting the bulk component from the spectra. Lines indicate the results of least-square fit to $F(X)$ (Reprinted with permission from Ref. 27).

halide/metal interfaces, so let us discuss the character of the MIGS in more detail.[27] First, anisotropy of MIGS was studied by polarization dependent NEXAFS. Figure 6 shows the polarization dependence of NEXAFS for LiCl/Cu(001) and LiCl/Ag(001). The X-ray incidence angle was 15, 55, and 90°. Intensity of the pre-peak was greater for grazing X-ray incidence (15°) than for normal incidence (90°). The intensity of the NEXAFS peak is proportional to $\cos^2\theta$, where θ is the angle between the electric vector of the X-ray and the transition moment of the excitation.[17] The electronic state that has a wave function oriented in the surface parallel (normal) direction is selectively detected for grazing (normal) X-ray incidence. Therefore, the observed polarization dependence results indicated that the MIGS had a p_z ($z \perp$ surface) like character, which was consistent with the above DFT calculation results.[26]

Second, the spatial distribution of MIGS in the surface normal direction is discussed in terms of decay length. The decay length was estimated according to the following procedure. First, the pre-peak of the film was extracted by subtracting the bulk component. Figure 7 shows the thickness dependence of the intensity of the pre-peak (not normalized by edge-jump) for LiCl/Cu(001) and Ag(001), together with that for KCl/Cu(001) and KCl/Ag(001). Here, we assumed that the probing depth of NEXAFS was much greater (typically >1000 nm) than the atomic scale, and the intensity of MIGS($f(x)$) at the distance x could be represented as $I_0\exp(-x/\lambda)$, where I_0 and λ were the intensity of MIGS at the interface and decay length, respectively. The intensity of MIGS ($F(X)$; film thickness X) observed by NEXAFS was, thus, represented as $I_0\lambda(1-\exp(-X/\lambda))$ by integrating $f(x)$ from 0 to X. By fitting the experimental data with $F(X)$, the decay length was determined to be 0.26 nm for LiCl/Cu(001), 0.29 nm for LiCl/Ag(001), 0.46 nm for KCl/Cu(001), and 0.41 nm for KCl/Ag(001), which indicated that the MIGS were indeed localized within a subnanometer regime of the interface. The result for the fitting is included in Fig. 7.

The decay length of MIGS depended on a kind of alkali halide, and did not depend on the metal. We discussed these facts using the finite square-well potential problem. The penetration depth of the wave function of the bound state is proportional to $\sqrt{V}$, where V is the height of the potential well measured from the Fermi level. Since MIGS originates from the metal wave function penetrating into an insulating side, the penetration depth of the wave function corresponds to the decay length of MIGS. The height of the potential in alkali halide/metal is the energy difference between the Fermi level and the valence band maximum. Assuming that the Fermi level is located at the center of the band gap, the height of the potential is half of the band gap energy. The band gap energy is 8.5 eV for KCl and 9.4 eV for LiCl, and hence, the penetration of wave function (decay length of MIGS) of KCl with smaller band gap energy was larger than that of LiCl. Because the height of the potential well depended less on the metal, the decay length of MIGS was independent of the metal.

We now focus on the spatial distribution of MIGS in the surface parallel direction. Both Cl K and K K edges NEXAFS provide information on the unoccupied Cl-p and K-p electronic densities of states. In forming a (001) fcc alkali halide film, each layer consists of the same number of cations and anions, and cations and anions align alternately. Therefore, the spatial distribution of MIGS in the surface parallel direction can be discussed by comparing the intensity of the MIGS peak in Cl edge and K edge NEXAFS for KCl film grown on a metal substrate. Figure 8 shows both Cl K and K K edges NEXAFS for KCl/Cu(001). The pre-peak originating from MIGS was clearly observed at the Cl edge, while the pre-peak was not observed at the K-edge. These NEXAFS results revealed that the MIGS were formed only at the anion site. On the other hand, the polarization dependent NEXAFS results showed that the MIGS have electron clouds extended along the surface normal direction. Considering these NEXAFS results and previous theoretical calculation results (Fig. 3 in Ref. 26), we could present a systematic view of the spatial distribution of MIGS for alkali halide/metal interface as seen in Fig. 9.

Localization of MIGS at the anion site can be discussed by

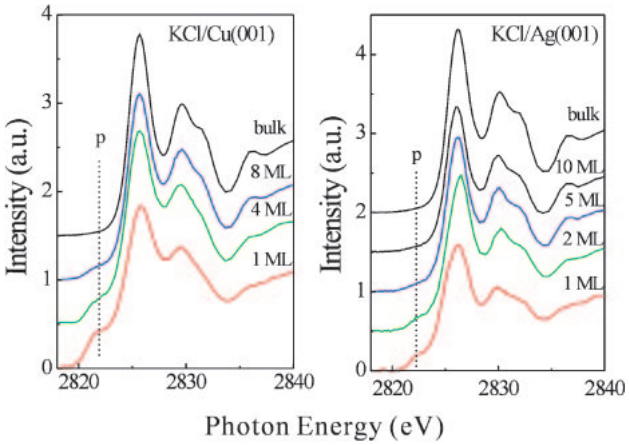

Fig. 8. The Cl K and K K edge NEXAFS spectra in KCl films grown on Cu(001) for various thicknesses of the KCl layer taken at the X-ray incidence angle of 15°, except the bottom one (normal incidence). All the spectra are normalized by their edge-jump (Reprinted with permission from Ref. 27).

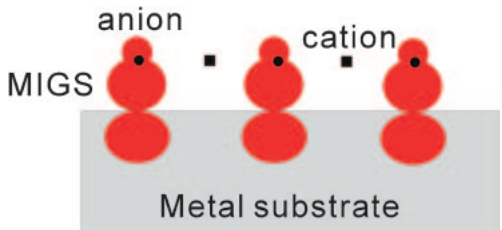

Fig. 9. Schematic view of the spatial distribution of MIGS for alkali halide/metal interface. The position of cation (box) and anion (circle) is shown in the figure.

considering the results of theoretical calculation.[29] Generally, MIGS can be divided into two groups: one having conduction band character and the other having valence band character in the insulator side of the interface. Noguera and Bordier have defined introduced E_{ZCP} to categorize the character of MIGS.[30] According to their theory, MIGS have conduction (valence) band character, when their energy is larger (smaller) than E_{ZCP}. On the other hand, charge transfer between the insulator and the metal is determined by the relative energy level of E_{ZCP} and Fermi energy (E_F). Charge transfer from the insulator to the metal (from the metal to the insulator) occurs if $E_{ZCP} > E_F$ ($E_{ZCP} < E_F$). Arita et al. have evaluated the charge transfer for various alkali halide/metal systems by ab initio calculations and have found that charge transfer from the insulator to the metal commonly occurs for alkali halide/metal systems.[29] This indicates that E_{ZCP} is higher than E_F for alkali halide/metal systems. Since E_{ZCP} is higher than E_F, MIGS, which are formed near E_F, has valence band (anionic) character.

3. Atomic and Electronic Structure of Polar MgO(111) Surface

3.1 Polar Surface. While the previous section, the insulator that was studied was an alkali halide, we now focus on an another insulator, metal oxides. In case of alkali halide/metal, a weak interaction between the film and substrate is essential for the epitaxial growth of alkali halide on metal surface. On the other hand, the interaction between oxide and metal is rather strong. Using this strong interaction, we fabricated novel atomic structures. In this section, we discussed the polar surface of MgO grown on metal substrates.

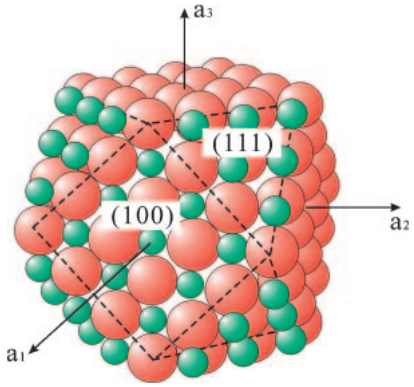

Fig. 10. Atomic geometry of the non-polar (100) and polar (111) faces of a rock salt crystal.

Polar surfaces have attracted wide attention not only for fundamental science but also for technological applications, because several interesting properties, such as novel catalytic activity, two-dimensional electron system, are expected for the polar surface. Figure 10 shows the atomic geometry of non-polar (100) and polar (111) faces of rock salt crystals schematically. The (111) surface consists of only one atomic species, either cations or anions, while the (100) surface consists of the same number of cations and anions. In a crystal with a rock salt structure, each atom is surrounded by six atoms of different species. The coordination number decreases to five for atoms on a (100) surface, while it changes to three for atoms on a (111) surface. Therefore, surface energy of the (111) face is much higher than that of the (100) face, which makes the (111) surface unstable.[31] In other words, alternate stacking of cation and anion layers forms a dipole layer along the [111] direction. Accumulation of the dipole layers should produce a macroscopic electric field, which causes the appearance of a flat (111) surface to be quite unpreferable in the rock salt structure compounds and the flat (111) surface does not occur in nature.

From a theoretical viewpoint, the macroscopic electric field in the polar surface can be cancelled either by surface reconstruction or by reduction of the effective charge of the surface layer. According to Wolf, the polar (111) surface of rock salt crystals would be stable under an octapole termination, which leads to formation of a 2×2 reconstruction on the (111) surface.[31] On the other hand, Tsukada and Hoshino pointed out that the change in charge state of surface atoms could stabilize the (111) surface of rock salt structure.[32] If the charge of the surface atoms is reduced to half of the bulk atoms, the macroscopic electric field would not appear. Using this information, several attempts to grow rock salt structure crystals with a polar surface have been performed so far. However, surface was p(2×2) reconstructed in many cases, and unreconstructed surfaces were only stable in the presence of some adsorbates.[33–37] There have been only a few studies on unreconstructed adsorbate-free (111) surfaces of a rock salt structure until now. Therefore, the electronic structure of the polar surface has

not been clear.

In the present study, we examined growth of a MgO thin film on Ag(111) by supplying Mg and O, alternately.[38,39] MgO has a rock salt structure with a lattice constant of 4.21 Å, while Ag has a fcc structure with a lattice constant of 4.09 Å. As the lattice misfit of MgO to Ag is only −2.9%, the first Mg layer is expected to become a template for the growth of the MgO film along the [111] direction. The commensurate bonding between Mg and Ag atoms at the interface might help alternate stacking of Mg and O layers, leading to a flat (111) surface.

3.2 Fabrication of MgO(111) Polar Surface on Ag(111). A MgO film was grown by alternate adsorption of Mg and O_2 on Ag(111) with a substrate temperature of 300 K. First, 1 ML (2 Å) Mg was deposited by evaporating high purity (99.98%) Mg onto Ag(111). The growth rate was monitored using a quartz crystal oscillator. The Mg film was dosed with 10 L O_2. Real-time observation of the crystallinity and orientation of films was done by RHEED. Surface compositions and the electronic structure of the grown films were investigated in situ by AES, EELS, and UPS.

The chemical state of Mg atoms and stoichiometry of the MgO film was examined by AES. Mg was completely oxidized and a stoichiometric MgO film was grown on Ag(111). Figures 11a–11d show the typical sequence of RHEED pattern during the growth at a substrate temperature of 300 K. The incident electron beam was parallel to the $[1\bar{1}0]$ azimuth of the substrate. The result of RHEED patterns indicated that the MgO film grew heteroepitaxially on Ag(111). The epitaxial orientation of the MgO film was determined to be $(111)_{MgO}//(111)_{Ag}$ and $[1\bar{1}0]_{MgO}//[1\bar{1}0]_{Ag}$. Half-order streaks did not appear during the growth, showing that the (1 × 1) unreconstructed MgO(111) film was grown on Ag(111). Streaks in RHEED patterns indicated that a rather flat (111) surface was obtained. The RHEED pattern became blurred with increasing film thickness, suggesting that the thick MgO(111) film was unstable.

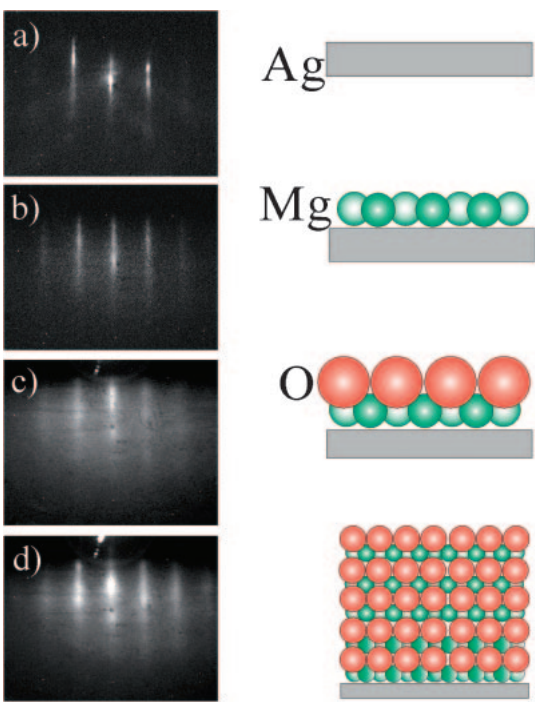

Fig. 11. A typical sequence of RHEED patterns and schematic models during the growth of the MgO film on Ag(111) at a substrate temperature of 300 K. a) Ag(111), b) 1 ML Mg/Ag(111), c) 2 ML MgO/Ag(111), d) 10 ML MgO/Ag(111). The incident beam was parallel to the $[1\bar{1}0]$ azimuth of the Ag(111) (Reprinted with permission from Ref. 38).

The in-plane lattice constant of the MgO(111) film was calculated from the spacing between streaks in the RHEED pattern. For the 10 ML thick MgO(111)/Ag(111), the in-plane lattice constant was determined to be 3.28 ± 0.03 Å, which was +10% larger than that of bulk one (2.97 Å). The in-plane lattice constant was 3.25 ± 0.03 Å for the 2 ML thick film and did not change with film thickness, indicating that the expansion was uniform throughout the epitaxial layer. The increase in the in-plane lattice constant leads to reduction of the surface electron density, which might help a decrease in the electrostatic energy of the MgO(111) film.

Having established the existence of the (1 × 1) unreconstructed MgO(111) film on Ag(111), we should discuss why this structure was stable in spite of the previously mentioned arguments on the instability of a polar surface of ionic crystals. In our previous study,[12] a single crystalline MgO(100) film grew heteroepitaxially on Ag(100) by evaporating MgO congruently from an electron beam evaporator (EB). On Ag(111), however, a MgO film could not grow heteroepitaxially by EB. Heteroepitaxial growth of a single crystalline MgO film was achieved by alternate adsorption of Mg and O_2 on Ag(111). These facts indicated that the strong interaction between Mg and Ag atoms played a decisive role in stabilizing the (1 × 1) MgO(111) film. The free energy of the interface (E_{inter}) is smaller for the case with coherent Mg–Ag bonds as compared with the case, in which fine particles with thermodynamically more stable {100} faces grow on Ag(111) without coherent Mg–Ag bonds. The structure of the grown film was determined to minimize the sum of the electrostatic energy of the film ($E_{electro}$) and E_{inter}. Here, it should be noted that $E_{electro}$ of a (111) film does not reach exorbitant values for ultrathin films, because $E_{electro}$ is proportional to the film thickness. Therefore, the gain in the interaction between Mg and Ag overcomes the disadvantage of the electrostatic energy, and the (1 × 1) unreconstructed MgO(111) film could be grown on Ag(111). In addition to the strong interaction with Mg atoms, the Ag substrate would play another important role for stabilization of the MgO(111) film. A MgO film was prepared by alternating the adsorption of Mg and O_2. Therefore, the film was unstable due to breakdown of charge neutrality, when the film thickness was an odd number (Mg top). On the metal substrate, however, an image charge was induced in the metal, helping stabilization of the film with odd layers.

3.3 Electronic Structure of Polar MgO(111) Surface. After preparing an unreconstructed polar MgO(111) surface, the electronic structure of this surface was investigated by EELS and UPS, comparing with that of a non-polar MgO(100) surface.[12] Absence of Ag LMM Auger peak in the 10 ML MgO(111)/Ag(111) meant that influences of the substrate were negligible in EELS and UPS, because their probing depth is smaller than or equal to that of AES. Figure 12 shows

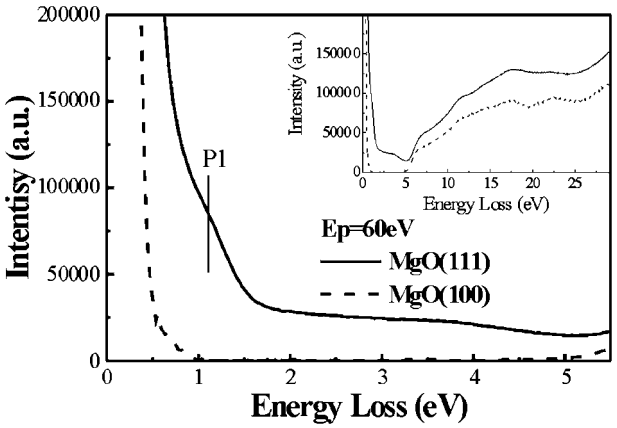

Fig. 12. EEL spectra of the polar MgO(111) surface (line). The primary electron energy was 60 eV. Spectra of MgO(100) surface is shown for comparison (dot line) (Reprinted with permission from Ref. 38).

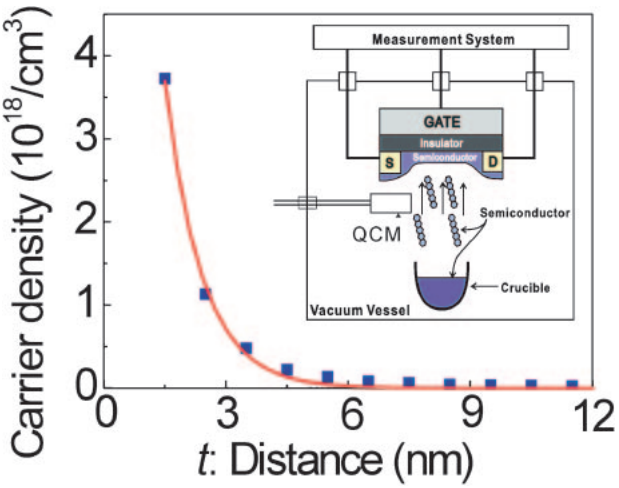

Fig. 13. Carrier density ($n(x)$) induced by electric field as a function of the distance (x) from the interface. (Inset) Schematic sample layout. The source (S)–drain (D) current was measured in-situ at various gate voltages.

the EELS of the MgO(111) surface measured with primary electron energy of 60 eV. For comparison, spectrum of the MgO(100) surface is also shown in the figure. The structure above 7 eV for MgO(111) was almost similar to that of MgO(100), showing that a stoichiometric MgO film grew on Ag(111). On the other hand, a difference appears in the structure below 5 eV between MgO(100) and (111). In contrast to MgO(100), the clear band gap region was not observed for MgO(111). In addition, the tail of the elastic peak became larger and a new peak (P1) appeared at 1.2 eV, indicating existence of the inelastically scattered electrons with small loss-energy. Since the AES signal indicative of Mg metal was not observed, the tail or the new peak did not originate from Mg aggregates in the MgO film. The finite DOS at the Fermi level was also observed for MgO(111) by UPS. The UPS and EELS results suggested that the MgO(111) surface was not an insulating surface but a semiconducting or metallic surface.

The semiconducting or metallic electronic structure of the MgO(111) surface can be explained in terms of Madelung potential. Compared to the binding energy of isolated ions, the binding energy of Mg^{2+} 3s orbital decreases, and the binding energy of O^{2-} 2p orbital increases by the Madelung potential in a crystal phase. Because of the decrease in the coordination number, the Madelung potential largely decreases for the (111) surface, compared with the (100) surface. Therefore, the band gap is reduced and the MgO(111) surface changes into a semiconductor or metallic surface. However, a possibility of certain new electronic state characteristic of the (111) surface cannot be excluded.

4. Chemical and Physical Properties of Well-Defined Nano Structures

4.1 Conductance of Well-Defined Nano Structures. In the previous section, we have discussed the fabrication of the well-defined nanostructures on metal surfaces. While atomic and electronic structures were investigated, the chemical and physical properties of the nanostructures have not been studied satisfactory. In this section, we investigated the chemical and physical properties of the well-defined nanostructures. Especially, attention was paid to electrical conductance. We studied the conductance of well-defined organic films and metal nanowires. In studies of the organic film, we investigated the distribution of the carriers in the pentacene, which grew on SiO_2 in layer-by-layer fashion at the initial stage of growth. As shown in the Fig. 13, the source (S)–drain (D) current in thin film transistors (TFT) was measured as a function of the film thickness of pentacene with a bottom-contact configuration. The gradual change in the conductivity was measured in-situ under the same condition at different gate voltages (V_G), avoiding the problem of specimen dependence, which is often encountered in the organic films due to the difference in grain size, crystallinity, interface state, etc. Figure 13 shows the obtained carrier density ($n(x)$) as a function of the distance (x) from the interface at various gate voltages. Most of carriers were localized in the first ML next to the interface.[40,41]

In the following, we mainly discuss the conductance of the well-defined metal nanowires. Fabrication and characterization of metal atomic wires have attracted attention due to their potential applications in future electronic devices. Electrical conductance through a metal nanowire on an atomic scale is expressed by $G = 2e^2/h \sum T_i$ where T_i is the transmission probability of the i-th conductance channel, e is the electron charge, and h is Plank's constant.[42] Conductance quantization depends on the atomic structure of a nanowire and the inherent properties of metals. For s-type metals, such as Au or Na, electron transport through a single atom occurs at a single channel with transmission close to unity, and thus, the conductance is quantized in the units of G_0. For other metals, other channels with different transmissions contribute to electron transport. Conductance at a monoatomic point contact of transition metals with partial occupied d orbitals is expected to be 1.5–3G_0 based on theoretical calculations.

While most of studies have been done in UHV at low temperature, in which fluctuation of environment is relatively small, preparation of stable metal ultra-small structures showing quantum conductance behavior at room temperature should be a challenging issue in this field. It has been demonstrated that electrochemical method can be used to solve the prob-

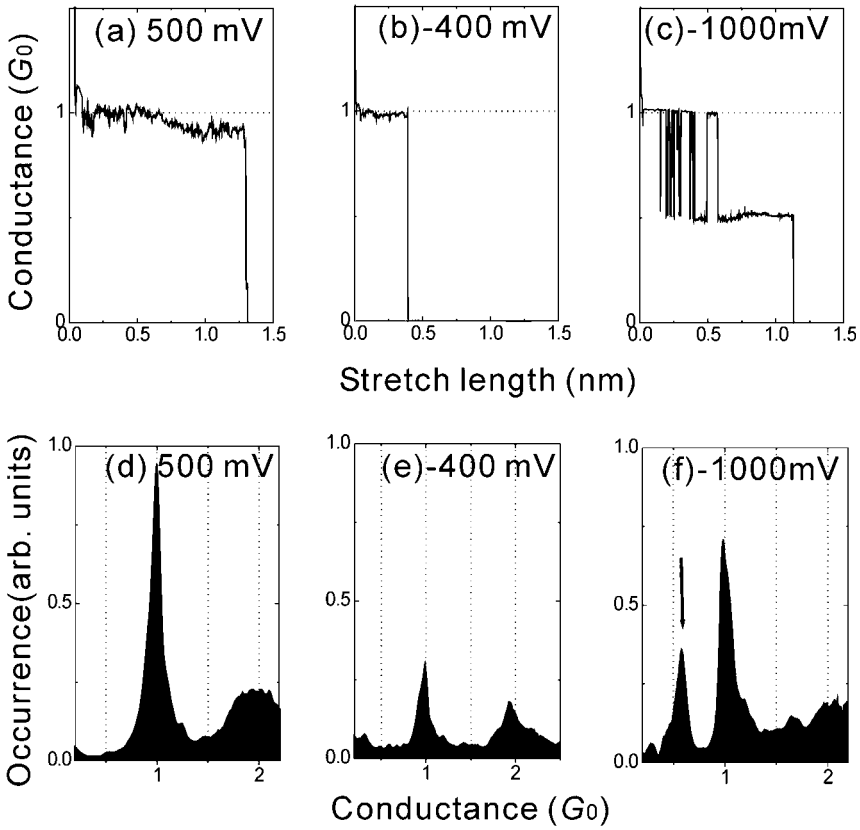

Fig. 14. (a–c) Conductance trace and (d–f) conductance histogram of gold nano wires in 0.1 M Na_2SO_4 at electrochemical potential of (a, d) +500 mV, (b, e) −400 mV, and (c, f) −1000 mV (Reprinted with permission from Ref. 46).

lem.[43,44] It is because potential energy of Fermi level, i.e., electronic structure, and adsorption or desorption of molecules or ions can be controlled by electrochemical potential in solution to stabilized the nanostructure. Thus, it is possible to fabricate novel metal nano structures, which cannot be prepared in UHV, and to control the electronic and geometrical structures on an atomic scale. In the present study, we have studied the quantum conductance behavior of the metal, i.e., Au, Fe, Co, Ni, Pd, nanoconstructions under electrochemical potential control.[45–47]

4.2 Conductance Switching Behavior in Au Mono Atomic Wire. The experimental setup was different from that of our previous studies in UHV. The experiments were performed in a four-electrode electrochemical cell mounted in a chamber that was filled with high purity N_2 gas to reduce the effect of oxygen. The gold nanowire was created by driving a STM tip in and out of contact with a gold substrate at a typical rate of 50 nm s^{-1} in the electrochemical cell. The tip was made of a gold wire (diameter 0.25 mm) coated with wax to eliminate ionic conduction. The gold substrate was Au(111) prepared by the frame annealing and quenching method. The electrochemical potential (ϕ) of the gold substrate and the tip was controlled using a potentiostat (Pico-Stat, Molecular Imaging Co.) with a Ag/AgCl reference electrode. A 0.50 mm diameter Pt wire was used as a counter electrode. For metal nanowire other than Au, metal was electrochemically deposited onto the surfaces of the STM tip and the substrate. Conductance of the gold nanowire was calculated on the basis of the observed current between the tip and the substrate at the potential difference of 20 mV.

Figure 14 shows the typical conductance traces and the conductance histogram of gold nanowires observed at $\phi = +500$, -400, and -1000 mV in 0.1 M Na_2SO_4. Each conductance histogram was obtained for a large number (over 3000) of individual conductance traces. The plateau of $1G_0$ stretched 1 nm in length at +500 mV (Fig. 14a). Since it has been shown that the conductance of the monoatomic gold contact is $1G_0$,[42,48,49] the 1 nm long $1G_0$ plateau proved the formation of the gold monoatomic wire in the present system. While a 2 nm long, gold monoatomic wire was fabricated at 4.2 K in UHV,[49] there are few reports of the formation of a monoatomic wire at room temperature. The present results proved that the electrochemical method made it possible to fabricate a stable gold monoatomic wire at room temperature in solution.

The length of the conductance plateau was dependent upon the electrochemical potential. As the potential was scanned from 500 mV to negative potential, the length decreased below −200 mV and reached a minimum at −400 mV. These electrochemical potential dependent changes in the stretch length were fully reversible. Increments in the length of the conductance plateau in positive and negative potential regimes could be explained by the adsorption of the sulfate anions[50] and that of hydrogen molecules on Au surface, respectively. This finding proves that the stability of the gold monoatomic wire could be controlled by the electrochemical potential.

In the negative potential regime, reversible transition of the conductance between $1G_0$ and 0.5–$0.7G_0$ was observed as shown in Fig. 14c. This conductance fluctuation resulted in

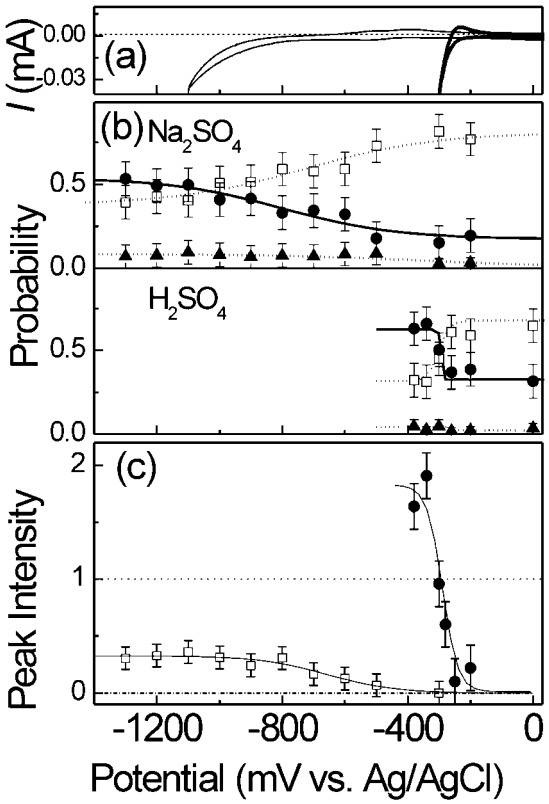

Fig. 15. (a) Voltammogram in 0.1 M Na_2SO_4 (thin line) and 50 mM H_2SO_4 (bold line). (b) The probability of each conductance trace in the presence of only fractional conductance step (triangle), only $1G_0$ conductance step (box), and both steps (filled-circle) as a function of electrochemical potential (ϕ). (c) The normalized fractional conductance intensity as a function of ϕ in Na_2SO_4 (box) and H_2SO_4 (filled-circle) (Reprinted with permission from Ref. 46).

the fractional conductance peaks in the conductance histogram (see Fig. 14f). The conductance fluctuation between two well-defined values strongly suggests the occurrence of a structural transition between two bistable states of the gold monoatomic wire. In solution, hydrogen evolution proceeds at the electrochemical potential in which the fractional value was observed. Therefore, hydrogen molecules and/or adsorbed hydrogen atoms may affect the evolution of the fractional conductance.

Figure 15 shows potential dependences of the reductive current due to the hydrogen evolution together with those of the occurrence of the fractional values in 0.1 M Na_2SO_4. Figure 15b shows the probability of the conductance trace in the presence of only a fractional conductance step, only a $1G_0$ conductance step, and both steps as a function of Φ. Figure 15c shows the intensity of the fractional conductance peak normalized by the $1G_0$ peak. With an increase in current due to the hydrogen evolution reaction, the probability of the conductance trace with the fractional conductance steps and the intensity of the fractional conductance peak increased. In the presence of the fractional conductance, both $1G_0$ and fractional conductance steps simultaneously appeared, suggesting that the fractional value originated from the conductance fluctuation. These results showed that evolved hydrogen induced the fractional conductance, which may reflect the occurrence of the transition between two bistable states of the gold monoatomic wire in the negative potential regime.

To confirm the effect of hydrogen on the fractional value, we studied electrochemical potential dependence of the conductance quantization behavior in acidic solution. The fractional conductance peak appeared in a potential regime more negative than $\phi = -200$ mV. It is noteworthy that the intensity of the fractional conductance peak was larger than that of $1G_0$ peak. In the solution with a lower pH (50 mM H_2SO_4), the onset potential of the hydrogen evolution shifted to more positive potential than that which occurred in the solution with a neutral pH (0.1 M Na_2SO_4), as shown in Fig. 15a. The occurrence of the fractional conductance shifted in accordance with that of the hydrogen evolution (see Fig. 15c). Dependence of the solution pH confirmed that the fractional conductance observed in solution originated from the structure stabilized by hydrogen.

The structure showing fractional conductance could be explained by the hydrogen-incorporated wire or dimerized wire. A recent theoretical calculation has shown that the incorporation of a hydrogen molecule in the gold monoatomic wire decreased conductance below $1G_0$.[51] On the other hand, a stretched single atom wire has a strong tendency to spontaneous dimerization—a predecessor for Peierls transition in extended 1D systems.[52] Theoretical calculation supports that the conductance of a dimerized gold wire is $0.4–0.6G_0$,[8] which is close to the observed values. Furthermore, fractional conductance feature and reversible conductance fluctuation between $1G_0$ and fractional conductance were reported for the gold nanowires under hydrogen dosing at 20 K in UHV.[53] If the dimerization is the origin of the fractional conductance, we could observe the Peierls transition of the 1D metal (monoatomic wire) at room temperature.

The present results clearly demonstrate the fabrication of a well-defined atomic structure with fractional conductance values controlled by the electrochemical potential.[46] In contrast to the UHV case, the intensity of the fractional conductance peak (stability) could be controlled by the electrochemical potential. Furthermore, the relative intensity of the fractional peak became stronger than that of the unit value (see Fig. 15c). The specific structure with $0.5–0.7G_0$ (fractional wire) became more stable than the structure with $1G_0$ (normal wire). It should be noted that the intensity of the fractional conductance feature does not exceed the $1G_0$ peak intensity even in the system in UHV at 20 K,[53] that is, fractional wire cannot be kept as the most energetically favorable structure. The present observation proved that structural bistability of gold monoatomic wires could be tuned by changing the electrochemical potential.

We have also studied the conductance of mechanically fabricated ferromagnetic metal (Ni and Pd) nanoconstructs while controlling the electrochemical potential and pH of the electrolyte.[45,47] The Ni and Pd monoatomic contact or monoatomic wire could be stabilized in solution at room temperature under the hydrogen evolution reaction. For Pd nanowire, the Pd wire was stretched 0.4 nm in length just before breaking, suggesting that at least two Pd atoms might contribute to the formation of the Pd wire.

5. General Conclusion

We have fabricated the well-defined nanostructures and investigate their chemical and physical properties. Among insulators, we focused on alkali halide and oxide. We have fabricated a well-defined alkali halide/metal interface and showed the existence of metal-induced gap states, characteristic of the metal/semiconductor or insulator interfaces. By growing MgO on Ag(111), we could fabricated the polar MgO(111) film, in which MgO(111) was unstable in bulk phase. We then studied the chemical and physical properties of this well-defined nanostructure. In case of Au monoatomic wires, we succeeded in controlling the switching behavior of conductance by the external perturbation, electrochemical potential.

While we and other groups have studied hetero-interface by various methods, there are still problems. Fabrication of the well-defined structures and investigation of their chemical and physical properties have been done separately. In order to improve the properties of the nanostructures drastically, fabricate and measurement of the properties should be done at the same time. At present, our focus has been on transistors (two-dimensional material) and single molecular device (one-dimensional material) based on our previous study. The transistor is based on the three layers of metal (gate), insulator, and semiconductor. In most transistors, insulating and semiconductor layers are polycrystalline, which leads to two problems. First, high electric field cannot be applied to semiconductor, because the insulating films would preferentially breakdown at the defects. Second, electrical conductance is inhibited by the grain boundary. On the other hand, we were able to fabricate single crystalline insulating films on metal substrates, and semiconductor films on insulating substrates.[9,10,12] Combing these techniques, we could fabricate all single crystalline transistors, whose performance would be much higher than conventional polycrystalline ones. On the other hand, single molecular electronic devices have attracted wide attention, since these devices represent the ultimate small electronic devices.[54] At present, electron transport through a molecule bridging two metal electrodes (molecular) has been studied by various methods. However, the number of molecules, and the atomic and electronic structures of the molecular junction are not clear. Recently, it was shown that IV curve provide the information about the electronic structure and vibration mode of the molecular junction, which can make clear the environment of the molecular junction.[55] By using these advanced methods, we determined the conductance of well-defined single molecule devices. Study in well-defined single molecular devices should also drastically improve the study of electronic devices.

Fabrication of the hetero-interface and investigation of its electronic structure were performed at the Professor Koichiro Saiki's laboratory (Graduate School of Frontier Sciences, the University of Tokyo). I would like to express my sincere gratitude to Prof. K. Saiki for his guidance, discussion, and to Professor H. Aoki, and Prof. A. Koma, Dr. R. Arita, Dr. G. Yoshikawa, Dr. S. Entani, and all other collaborators in Prof. K. Saiki's laboratory. The work was supported by a Grant-in-Aid for Scientific Research and Special Coordination Fund (No. 14GS0207) from MEXT. The NEXAFS measurements were performed under the approval of Photon Factory Program Advisory Committee (PF-PAC). The investigation of the metal nano wire was performed at the Professor Kei Murakoshi's laboratory (Graduate School of Science, Hokkaido University). I also would like to express my sincere gratitude to Prof. K. Murakoshi for his guidance, discussion, and all other collaborators in Prof. K. Murakoshi's laboratory. The work was supported by a Grant-in-Aid for Scientific Research A (No. 16205026) and Grant-in-Aid for Scientific Research on Priority Areas (No. 17069001) from MEXT.

References

1 A. Zangwill, *Physics at Surfaces*, Cambridge University Press, **1988**.
2 M. Haruta, *Chem. Rec.* **2003**, *3*, 75.
3 K. Saiki, *Appl. Surf. Sci.* **1997**, *113–114*, 9.
4 M. Kiguchi, K. Saiki, A. Koma, *Surf. Sci.* **2000**, *470*, 81.
5 M. Kiguchi, S. Entani, K. Saiki, A. Koma, *Surf. Sci.* **2003**, *523*, 73.
6 W. Shockley, *Bell Syst. Tech. J.* **1949**, *28*, 435.
7 L. Esaki, R. Tsu, *IBM Research Note*, RC-2418, **1969**.
8 K. Saiki, T. Kono, K. Ueno, A. Koma, *Rev. Sci. Instrum.* **2000**, *71*, 3478.
9 M. Kiguchi, K. Saiki, T. Sasaki, Y. Iwasawa, A. Koma, *Phys. Rev. B* **2001**, *63*, 205418.
10 M. Kiguchi, S. Entani, K. Saiki, H. Inoue, A. Koma, *Phys. Rev. B* **2002**, *66*, 155424.
11 R. Smoluchowski, *Phys. Rev.* **1941**, *60*, 661.
12 M. Kiguchi, T. Goto, K. Saiki, T. Sasaki, Y. Iwasawa, A. Koma, *Surf. Sci.* **2002**, *512*, 97.
13 M. Kiguchi, S. Entani, K. Saiki, G. Yoshikawa, *Appl. Phys. Lett.* **2004**, *84*, 3444.
14 M. Kiguchi, G. Yoshikawa, K. Saiki, *J. Appl. Phys.* **2003**, *94*, 4866.
15 G. Yoshikawa, M. Kiguchi, S. Ikeda, K. Saiki, *Surf. Sci.* **2004**, *559*, 77.
16 M. Kiguchi, H. Inoue, K. Saiki, T. Sasaki, Y. Iwasawa, A. Koma, *Surf. Sci.* **2003**, *522*, 84.
17 *NEXAFS Spectroscopy*, ed. by J. Stöhr, Springer-Verlag, New York, **1992**.
18 M. Kiguchi, T. Yokoyama, S. Terada, M. Sakano, Y. Okamoto, T. Ohta, Y. Kitajima, H. Kuroda, *Phys. Rev. B* **1997**, *56*, 1561.
19 M. Kiguchi, T. Yokoyama, D. Matsumura, H. Kondoh, T. Ohta, Y. Kitajima, *Phys. Rev. B* **1999**, *60*, 16205.
20 M. Kiguchi, T. Yokoyama, D. Matsumura, H. Kondoh, O. Endo, T. Ohta, *Phys. Rev. B* **2000**, *61*, 14020.
21 T. Ohta, P. M. Stefan, M. Nomura, H. Sekiyama, *Nucl. Instrum. Methods Phys. Res., Sect. A* **1986**, *246*, 373.
22 M. Funabashi, M. Nomura, Y. Kitajima, T. Yokoyama, T. Ohta, H. Kuroda, *Rev. Sci. Instrum.* **1989**, *60*, 1983.
23 S. A. Flodström, C. W. B. Martinsson, *Surf. Sci.* **1982**, *118*, 513.
24 S. Louie, M. Cohen, *Phys. Rev. B* **1976**, *13*, 2461.
25 J. Tersoff, *Phys. Rev. Lett.* **1984**, *52*, 465.
26 M. Kiguchi, R. Arita, G. Yoshikawa, Y. Tanida, M. Katayama, K. Saiki, A. Koma, H. Aoki, *Phys. Rev. Lett.* **2003**, *90*, 196803.
27 M. Kiguchi, G. Yoshikawa, S. Ikeda, K. Saiki, *Phys. Rev. B* **2005**, *71*, 153401.
28 M. Kiguchi, R. Arita, G. Yoshikawa, Y. Tanida, S. Ikeda,

S. Entani, I. Nakai, H. Kondoh, T. Ohta, K. Saiki, H. Aoki, *Phys. Rev. B* **2005**, *72*, 75446.
29 R. Arita, Y. Tanida, K. Kuroki, H. Aoki, *Phys. Rev. B* **2004**, *69*, 115424.
30 C. Noguera, G. Bordier, *J. Phys. III* **1994**, *4*, 1851.
31 D. Wolf, *Phys. Rev. Lett.* **1992**, *68*, 3315.
32 M. Tsukada, T. Hoshino, *J. Phys. Soc. Jpn.* **1982**, *51*, 2562.
33 A. Barbier, C. Mocuta, H. Kuhlenbeck, K. F. Peters, B. Richter, G. Renaud, *Phys. Rev. Lett.* **2000**, *84*, 2897.
34 R. Plass, K. Egan, C. Collazo-Davila, D. Grozea, E. Landree, L. D. Marks, M. Gajdardziska-Josifovska, *Phys. Rev. Lett.* **1998**, *81*, 4891.
35 M. A. Langell, C. L. Berrie, *Surf. Sci.* **1994**, *320*, 25.
36 P. A. Cox, A. A. Williams, *Surf. Sci.* **1985**, *152–153*, 791.
37 K. Saiki, A. Goda, A. Koma, *Jpn. J. Appl. Phys.* **1997**, *36*, L55.
38 M. Kiguchi, S. Entani, K. Saiki, T. Goto, A. Koma, *Phys. Rev. B* **2003**, *68*, 115402.
39 R. Arita, Y. Tanida, S. Entani, M. Kiguchi, K. Saiki, H. Aoki, *Phys. Rev. B* **2004**, *69*, 235423.
40 M. Kiguchi, M. Nakayama, T. Shimada, K. Saiki, *Phys. Rev. B* **2005**, *71*, 035332.
41 M. Kiguchi, M. Nakayama, K. Fujiwara, K. Ueno, T. Shimada, K. Saiki, *Jpn. J. Appl. Phys.* **2003**, *42*, L1408.
42 N. Agraït, A. L. Yeyati, J. M. van Ruitenbeek, *Phys. Rep.* **2003**, *377*, 81.
43 C. Shu, C. Z. Li, H. X. He, A. Bogozi, J. S. Bunch, N. J. Tao, *Phys. Rev. Lett.* **2000**, *84*, 5196.
44 J. L. Li, T. Kanzaki, K. Murakoshi, Y. Nakato, *Appl. Phys. Lett.* **2002**, *81*, 123.
45 M. Kiguchi, T. Konishi, K. Murakoshi, *Appl. Phys. Lett.* **2005**, *87*, 043104.
46 M. Kiguchi, T. Konishi, K. Murakoshi, *Phys. Rev. B* **2006**, *73*, 125406.
47 M. Kiguchi, K. Murakoshi, *Appl. Phys. Lett.* **2006**, *88*, 253112.
48 H. Ohnishi, Y. Kondo, K. Takayanagi, *Nature* **1998**, *395*, 780.
49 A. I. Yanson, G. R. Bollinger, H. E. van den Brom, N. Agrait, J. M. van Ruitenbeek, *Nature* **1998**, *395*, 783.
50 H. Uchida, M. Hiei, M. Watanabe, *J. Electroanal. Chem.* **1998**, *452*, 97.
51 R. N. Barnett, H. Hakkinen, A. G. Scherbakov, U. Landman, *Nano Lett.* **2004**, *4*, 1845.
52 M. Okamoto, K. Takayanagi, *Phys. Rev. B* **1999**, *60*, 7808.
53 S. Csonka, A. Halbritter, G. Mihály, E. Jurdik, O. I. Shklyarevskii, S. Speller, H. van Kempen, *Phys. Rev. Lett.* **2003**, *90*, 116803.
54 M. A. Reed, C. Zhou, C. J. Muller, T. P. Burgin, J. M. Tour, *Science* **1997**, *278*, 252.
55 R. H. M. Smit, Y. Noat, C. Untiedt, N. D. Lang, M. C. van Hemert, J. M. van Ruitenbeek, *Nature* **2002**, *419*, 906.

Manabu Kiguchi was born in Tokyo in 1972. He graduated from the Department of Chemistry, Faculty of Science, the University of Tokyo in 1995. He received the M.Sci. (1997), and the Ph.D. (2000) from the University of Tokyo. In 1999, he joined Professor Koichiro Saiki's group as a research associate at the University of Tokyo. He studied the atomic and electronic structure of the thin films on metal substrates. In 2004, he joined Professor Kei Murakoshi's group as a lecturer at Hokkaido university. His current researches have focused on fabrication of metal and molecular nanowire in solution.